Monte Carlo Simulations of Phase Transitions in ^{4}He-^{3}He Films

Brianna Dillon[1,2] and Richard Scalettar[2]
[1]*Physics Department, Grove City College, Grove City, PA 16127*
[2]*Physics Department, University of California, Davis, CA 95616*

The vector Blume-Capel model in two dimensions was studied on a square lattice using Monte Carlo simulations. We obtained a complete phase diagram showing a Kosterlitz-Thouless transition and a first order hysteresis region, and located the tricritical point. The phase diagram was consistent across two lattice sizes and two runtimes, and with the few individual data points found in the literature.

I. Introduction

We all are familiar with "everyday" phase transitions – freezing, melting, condensation, vaporization, etc. Phase transitions are of particular interest to scientists because they go against our usual expectation that a small change in a system's environment will enact a small change in the system's properties. For instance, in melting water, changing the temperature 0.01º from 31.99º F to 32.00º F results in a dramatic change – the solid ice becomes liquid. An even more interesting phase transition is the superfluid phase transition. Superfluidity is a special liquid phase in which the liquid has zero viscosity, meaning it flows without resistance. Superfluid phase transitions occur at very low temperatures. For instance, bulk ^{4}He transitions from a normal fluid to a superfluid as its temperature is decreased below its critical temperature of 2.17 K. Another isotope of helium, ^{3}He, becomes superfluid at even lower temperatures. The purpose of my project was to study how the superfluid phase transition of a ^{4}He film is affected by the addition of ^{3}He. This has been studied experimentally,[1-2] but I did a simulation study, using a two dimensional model to simulate the mixture film. The ultimate goal was to obtain a phase diagram showing how the system's critical temperature was affected by the quantity of ^{3}He added. S. Romano and others have also done simulation studies of this model, although only for a few specific parameters;[3-7] I will compare my results with their data points.

II. Model and Simulation Measurements

The model studied was the vector Blume-Capel model. In this model, the film is represented by a square lattice of sites which carry a continuous spin variable θ, which varies from 0 to 2π. This spin variable represents the order parameter for the superfluid ^{4}He. Additionally, the sites may be either occupied or vacant, as indicated by the variable *t*, which equals 1 if occupied and 0 if vacant. In the context of our study, an occupied site represents a ^{4}He atom, while a "vacant" site represents a ^{3}He atom. The Hamiltonian of the entire system is given by eqn 1:

$$H = -J \sum_{<i,j>} t_i t_j \cos(\theta_i - \theta_j) + D \sum_i t_i \qquad (1)$$

In the first term, J is a coupling constant for the spins and the sum is over nearest-neighbor pairs with periodic boundary conditions. For our simulation, we set J to be the unit of energy. The second term accounts for the number of vacancies present. At large negative values of D there are no vacancies and the model becomes the Planar Rotator model, representing pure ^{4}He; increasing D increases the number of vacancies, i.e. the amount of ^{3}He. At low temperatures, the system will tend to order itself with spins aligned parallel, indicating it is in the superfluid phase. At high temperatures, the spins orient themselves randomly, and the system is a normal fluid. In two dimensions, it is actually not possible for the system to obtain long range superfluid order (meaning the order extends through the whole sample), as it can in three dimensions. However, a subtle phase transition may still occur, called a Kosterlitz-Thouless transition.

I simulated this model using Monte Carlo with the Metropolis condition $e^{-\Delta E/T}$. Two Monte Carlo steps were done in each measurement cycle, one for the spin variables and one for the vacancy variables. The simulation was run in two ways. First, D was set constant, and the temperature was varied from lowest to highest, with each temperature starting with a new spin configuration. Second, temperature was held constant while D was varied first increasing then decreasing back to the initial value, with each increment of D starting with the spin configuration the previous value ended with. Each method was used to obtain part of the phase diagram, as I will discuss later.

After a certain number of Monte Carlo sweeps over the lattice in which the system was allowed to equilibrate, various thermodynamic quantities were measured within measurement sweeps after the Monte Carlo steps. To ensure that the values used in computing averages were statistically uncorrelated, the measurements were binned. The average values of the

bin contents were then used to compute overall average values and standard deviation. The quantities measured were the average energy per site *E*, and specific heat *C*, given by eqns 2 and 3:

$$\langle E \rangle = \frac{1}{L^2} \sum_{i=1}^{L^2} E_i \tag{2}$$

$$C = L^2 \frac{\langle E^2 \rangle - \langle E \rangle^2}{T^2} \tag{3}$$

where L is the lattice size and T is the temperature of the system.

Although a superfluid is not a magnet, it is similar to one in that it is an ordered system. That is, the parallel spins which in our model represent the ordered superfluid phase could, in a different context, be used to represent parallel magnetic domains. Therefore, by measuring the superfluid's "magnetization per site" *M* and magnetization susceptibility χ_M (eqns 4 and 5), we can understand how the system is ordered. To see how the number of vacancies varied, I also measured the vacancy concentration *X* and concentration susceptibility χ_X (eqns 6 and 7).

$$M = \frac{1}{L^2} \sqrt{\left(\sum_{i=1}^{L^2} M_i^x \right)^2 + \left(\sum_{i=1}^{L^2} M_i^y \right)^2} \quad \text{where} \quad M_i^x = \cos\theta_i \ \text{ and } \ M_i^y = \sin\theta_i \tag{4}$$

$$\chi_M = L^2 \frac{\langle M^2 \rangle - \langle M \rangle^2}{T} \tag{5}$$

$$X = \frac{1}{L^2} \sum_{i=1}^{L^2} (1 - t_i) \tag{6}$$

$$\chi_X = L^2 \frac{\langle X^2 \rangle - \langle X \rangle^2}{T} \tag{7}$$

The last quantity to be measured was the helicity modulus, or spin stiffness, of the system. The helicity modulus measures how correlated the spins are; it varies between 0, indicating no correlation, and 1, indicating high correlation. It is found by taking the second derivative of the free energy with respect to a spin twist Δ, as given in eqn 8:

$$\Upsilon = \frac{\partial^2 f}{\partial \Delta^2} = \frac{1}{T} \left[\left\langle \sum_{<i,j>:x} t_i t_j \sin(\theta_i - \theta_j) \right\rangle^2 - \left\langle \left(\sum_{<i,j>:x} t_i t_j \sin(\theta_i - \theta_j) \right)^2 \right\rangle \right] + \left\langle \sum_{<i,j>:x} t_i t_j \cos(\theta_i - \theta_j) \right\rangle \tag{8}$$

where the sums are over nearest neighbor pairs in the x-direction only. Since the spins tend to align themselves parallel at low temperatures, a small change in one spin will induce the rest to line up accordingly; therefore we expect that Υ = 1 at low temperatures. Likewise, we expect Υ = 0 at high temperatures since the spins orient themselves irrespective of their neighbors.

III. Obtaining the Phase Diagram

To locate the phase transition, I first looked for the intersection of Υ vs. T with the line $(2/\pi)T$, which gives the critical temperature T_c for a given value of D. For this I used the constant D, variable T method at successive values of D. Figure 1 shows a representative sample of plots. One can easily see that the critical temperature decreases with increasing D; that is, with increasing vacancies. Also, as D is increased, the inflection of the helicity modulus becomes increasingly vertical, indicating a shift from a smoothly varying Kosterlitz-Thouless transition toward a first-order transition.

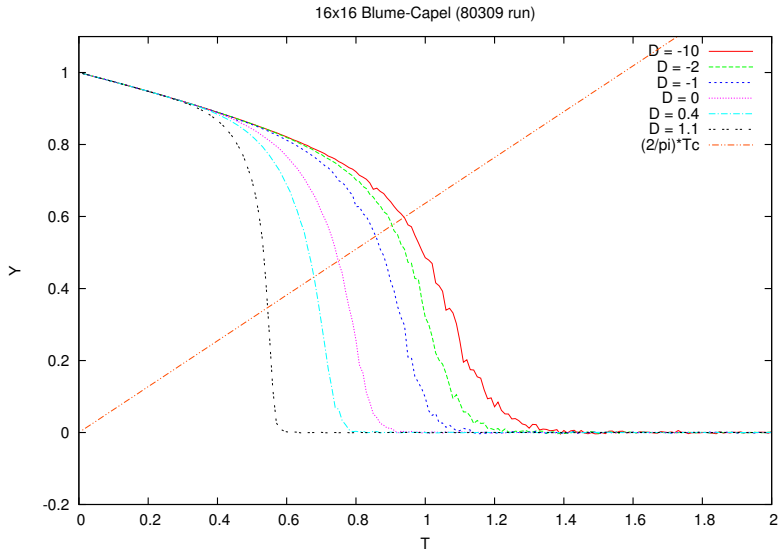

Figure 1: Helicity modulus vs. temperature for a 16x16 lattice with 50,000 equilibration cycles and 100,000 measurement cycles, and D = -10, -2, -1, 0, 0.4, and 1.1.

Unfortunately, this technique produces only a partial phase diagram, as shown in Figure 2, because around D = 1.3 the system contains only vacancies and the helicity modulus is therefore zero. Moreover, the phase boundary levels out horizontally. Thus looking at a different quantity would be of no use, because I was doing a horizontal sweep across temperature.

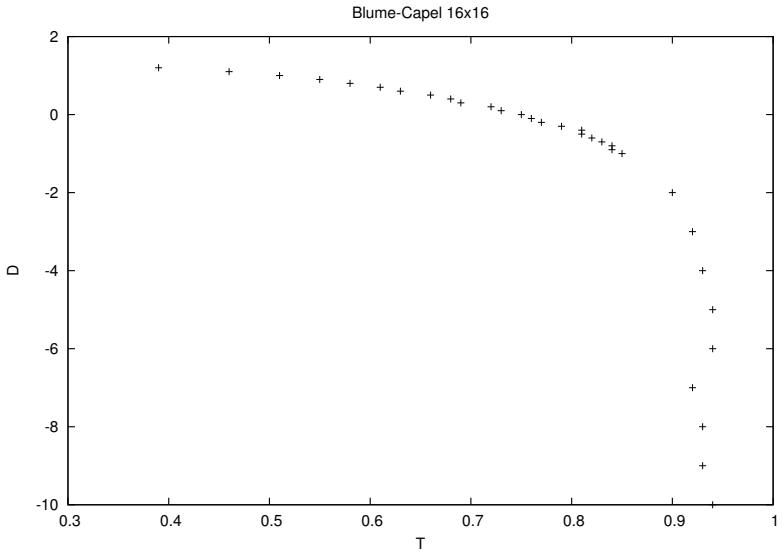

Figure 2: Partial phase diagram for 16x16 lattice with 10,000 equilibration cycles and 10,000 measurement cycles. The phase boundary shown is from helicity modulus analysis only.

To fill out the phase diagram at temperatures lower than 0.4K, I looked at the vacancy concentration vs. D, given by the constant T, variable D method. I chose to look at the vacancy concentration because, from the partial phase diagram already obtained, I knew that in doing a vertical scan, the simulation would be moving from a region of nearly no vacancies to a region of almost all vacancies, and back again. Thus the change in vacancy concentration at the phase boundary would be a distinct one. We also suspected that at low temperatures the system was undergoing a first order transition, as hinted at in the helicity modulus plots obtained earlier, and thus might be subject to hysteresis. For this reason the simulation was run over a cycle of values, from low D to high D and back to the initial low value, rather than just one direction. Figure 3 shows the hysteresis effect very clearly; the hysteresis begins somewhere between T = 0.5 and T = 0.4. The hysteresis loop widens as the temperature is lowered. Consequentially, two values of D_c were obtained for each temperature at which the simulation was run.

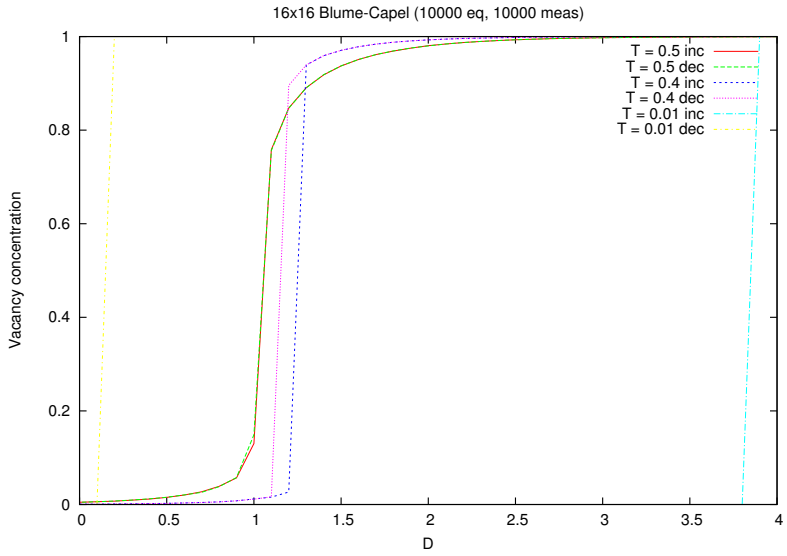

Figure 3: Hysteresis loops for T = 0.5, 0.4, and 0.01 on a 16x16 lattice with 10,000 equilibration cycles and 10,000 measurement cycles. Note that the increasing and decreasing sweeps for T = 0.5 actually overlap; there is no hysteresis at this temperature.

Notice that in Figure 3 the maximum separation is nearly 4D at T = 0.01, the lowest temperature measured. This is what we expected. When $T \approx 0$, the most stable state at $D < 0$ is with all sites occupied and spins aligned. If we try to add a vacancy, the energy cost is $\Delta E = +4J - D$, since we are destroying four bonds to add the vacancy. The acceptance probability for this move, $e^{-\Delta E/T}$, is very small since $T \approx 0$, thus such a move is always rejected. When ΔE changes sign as we increase D, however, this changes dramatically. Now $e^{-\Delta E/T}$ is very large, and all vacancy additions are accepted. This change of sign occurs when $\Delta E = 0$, i.e. when $D/J = 4$ (see light blue line in Fig. 3). Similarly, if we start in a region with all vacancies, the addition of a spin is very unlikely because $e^{-\Delta E/T}$ is very small. However as we decrease D, when ΔE changes sign all spin additions are accepted; in this case when $D/J = 0$ (see yellow line in Fig. 3). Therefore, at T very close to zero, we expect the hysteresis spread to be about 4D, which we did indeed observe.

The onset of hysteresis signifies the change from a Kosterlitz-Thouless transition to a first-order transition, which is called the tricritical point. To locate the tricritical point more precisely, the simulation was run at finer temperature increments. As seen in Figure 4, the tricritical point for this particular simulation was T = 0.42; below this temperature the transition is first order.

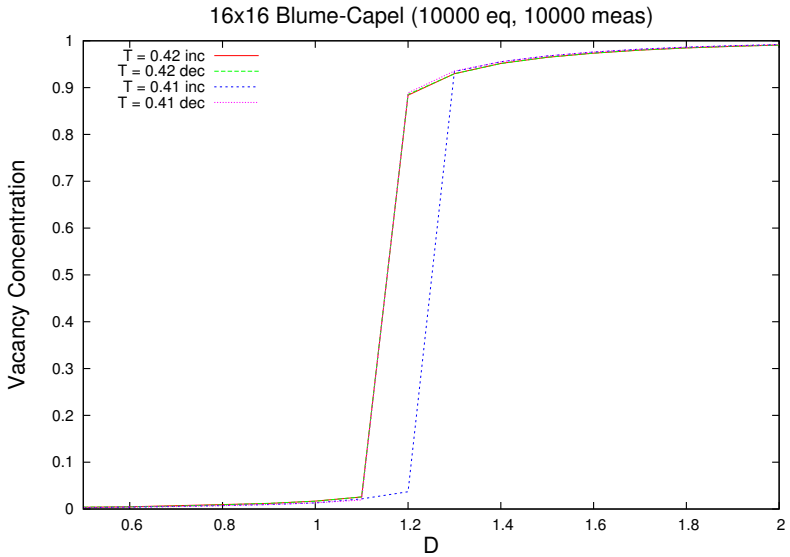

Figure 4: More detailed location of tricritical point on a lattice with same conditions as Fig 3. At T = 0.42, there is no hysteresis, but at T = 0.41 there is. Thus the tricritical point is T = 0.42 for this lattice.

IV. Results and Analysis

Simulations were run on a 16x16 lattice at two different runtimes, as well as a 32x32 lattice. The phase diagram for the longer 16x16 run is shown as a representative example (Fig 5).

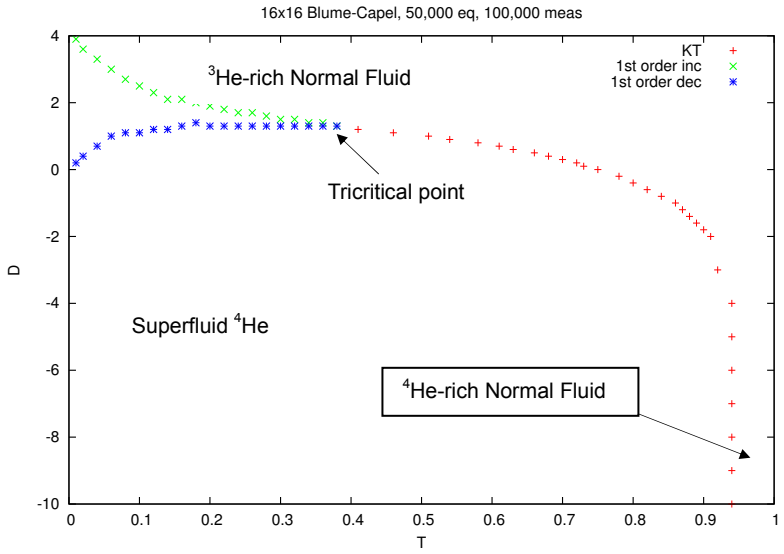

Figure 5: Complete phase diagram for a 16x16 lattice with 50,000 equilibration cycles and 100,000 measurement cycles. Red indicates the Kosterlitz-Thouless transition; green and blue are the 1st order hysteresis loop results.

At D < -4, the model is essentially the Planar Rotator model, with the critical temperature 2-5% off from the known value of $T_{PR\infty} = 0.89$ for an infinite lattice. With larger lattice sizes our results approach this value. The phase transition in this region is a Kosterlitz-Thouless transition from a normal fluid with high ^{4}He concentration to superfluid ^{4}He. At low temperatures, the system undergoes a first order transition from superfluid ^{4}He to ^{3}He-rich normal fluid, and you can clearly see the 4D/J spread at T = 0. The tricritical point for this system was found to be $0.38 < T_{tricrit} < 0.42$ depending on lattice size and runtime. Table 1 summarizes our results.

Lattice Size	**16x16**	**16x16**	**32x32**
Equilibration cycles	10,000	50,000	200,000
Measurement cycles	10,000	100,000	400,000
T_{PR}	0.94	0.94	0.92
$T_{tricrit}$	0.42	0.38	0.42

Table 1: Table of the conditions for the three simulations done, and the location of the critical temperature at the planar rotator limit (T_{PR}) and the tricritical point ($T_{tricrit}$) for each.

Comparing the two 16x16 simulations (Fig 6), we see that they line up very nicely; the biggest difference is that the tricritical point for the longer runtime is shifted to lower temperature (see Table 1). Thus, while a longer runtime did yield a smoother phase boundary, I still get good results out of a short runtime. This will be convenient should I wish to run simulations on lattice sizes even larger than 32x32; I can keep the runtime within a reasonable length without sacrificing much accuracy.

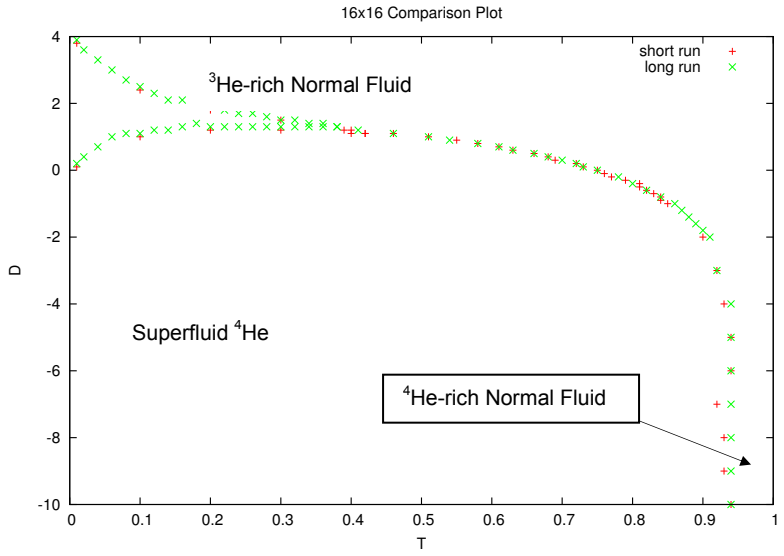

Figure 6: Comparison of the phase diagrams for a 16x16 lattice with 10,000 equilibration cycles and 10,000 measurement cycles (red) and with 50,000 equilibration cycles and 100,000 measurement cycles (green).

Comparing the 32x32 simulation with the long 16x16 simulation (which had a runtime of proportionate length), we see that again, they overlap closely (Fig 7). The greatest difference is T_{PR}; as mentioned previously, $T_{PR} \rightarrow T_{PR\infty}$ with larger lattice size.

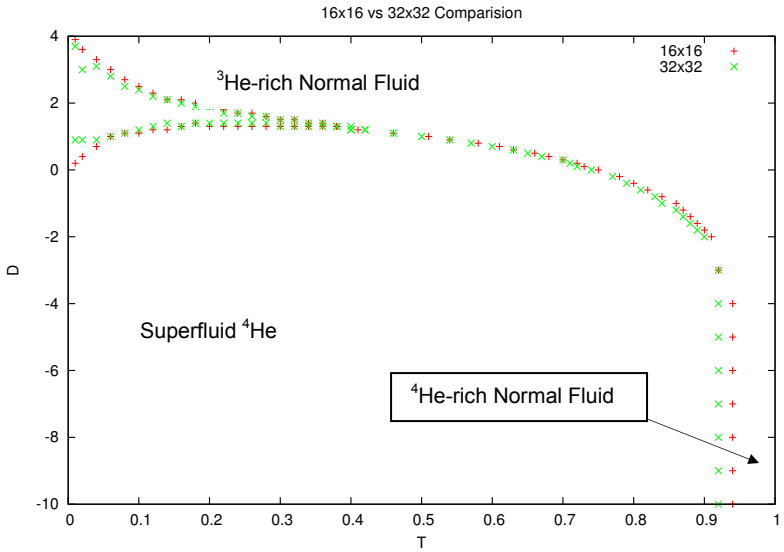

Figure 7: Comparison of phase diagrams for a 16x16 lattice with 50,000 equilibration cycles and 100,000 measurement cycles (red) and a 32x32 lattice with 200,000 equilibration cycles and 400,000 measurement cycles (green).

In fact, if we relate T_{PR} to inverse lattice size and assume a linear fit, we can extrapolate our results to determine what our simulation would give at infinite lattice size[8,9]:

$$T_{PR}\left(\frac{1}{L}\right) = \frac{0.94 - 0.92}{(1/16) - (1/32)}\left(\frac{1}{L} - \frac{1}{32}\right) + 0.92 \quad \rightarrow \quad T_{PR}\left(\frac{1}{L}\right) = 0.64\left(\frac{1}{L}\right) + 0.9$$

Thus at $L = \infty$, $T_{PR} = 0.9$ for our simulations, which is only about 1% error.

Though to the best of our knowledge no one has yet produced a full phase diagram for the Blume-Capel model, Romano and others have studied this model for specific values of D.[7] Our phase diagram results are in good agreement with his points. His results are shown plotted atop my phase diagrams in Figure 8.

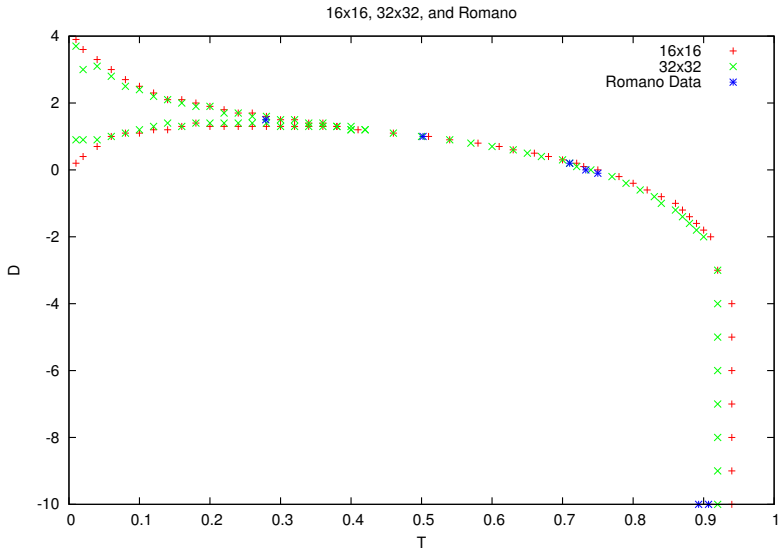

Figure 8: Comparison of the phase diagrams shown in Fig 7 (colors the same) with S. Romano's simulation results (blue)[7]

V. Conclusion

We simulated the vector Blume-Capel model using Monte Carlo on a two-dimensional square lattice. Simulations were done on 16x16 and 32x32 lattices, with equilibrations ranging from 10,000 to 200,000 cycles, and measurements done over 10,000 to 400,000 cycles. Our results were consistent with each other, differing only in T_{PR}, which decreased with increasing lattice size as expected, and in the location of the tricritical point. Additionally, our results were consistent with the few data points found in the literature. Extrapolating our simulation results, we obtain $T_{PR} = 0.90$ for an infinite lattice, which is within 1% of the true value. The tricritical point was found to be between T = 0.38 and T = 0.42; future work will focus on pinpointing the tricritical point's location more precisely.

Acknowledgements

I would like to acknowledge the excellent guidance and support of my advisor, Dr. Richard Scalettar, and of Dr. Simone Chiesa, who was a secondary mentor. This work was supported by the NSF through the 2009 Research Experience for Undergraduates at the University of California, Davis.

References

[1] G. A. Csáthy and M. H. W. Chan, Phys. Rev. Lett. **87**,045301 (2001)
[2] G. A. Csáthy, E. Kim, and M. H. W. Chan, Phys. Rev. Lett. **88**,045301 (2002)
[3] S. Romano, Int. J. Mod. Phys. B **13**, 191 (1999)
[4] S. Romano and O. Sokolovskii, Phys. Rev. B **61**, 11379 (2000)
[5] H. Chiamati and S. Romano, Phys. Rev. B **72**, 064424 (2005)
[6] H. Chiamati and S. Romano, Phys. Rev. B **72**, 064444 (2005)
[7] H. Chiamati and S. Romano, Phys. Rev. B **75**, 184413 (2007), particularly Table 1.
[8] A. Maciolek, M. Krech, and S. Dietrich, Phys. Rev. E **69**, 036117 (2004)
[9] R. T. S. Freire, S. J. Mitchell, J. A. Plasak, and D. P. Landau, Phys. Rev. E **72**, 056117 (2005)